International Journal of Solids and Structures, in press

Nonlinear Multiscale Modeling of Polymer Materials

P.K. Valavala
Department of Mechanical Engineering – Engineering Mechanics
Michigan Technological University
1400 Townsend Drive
Houghton, MI 49931

T.C. Clancy
National Institute of Aerospace
100 Exploration Way
Hampton, VA 23666

G.M. Odegard*
Department of Mechanical Engineering – Engineering Mechanics
Michigan Technological University
1400 Townsend Drive
Houghton, MI 49931

T.S. Gates
Mechanics of Structures and Materials Branch
MS 188E
NASA Langley Research Center
Hampton, VA 23681

Abstract

In this study, a hyperelastic multiscale modeling technique is used to predict elastic properties of polycarbonate and polyimide polymer systems using a set of widely accepted atomistic force fields. The model incorporates molecular simulations and a nonlinear, continuum mechanics-based, constitutive formulation that incorporates the behavior of the polymer materials as predicted from molecular simulations. The predicted properties of the polymers using multiple force fields are compared to experimentally-measured values. Both static and dynamic molecular simulations are performed using Molecular Mechanics energy minimizations and Molecular Dynamics simulation techniques, respectively. The results of this study indicate that static molecular simulation is a useful tool to predict the bulk-level nonlinear mechanical behavior of polymers for finite deformations. It is found that the AMBER force field yields the most accurate predicted mechanical and physical properties of the modeled polymer systems compared to the other force fields used in this study.

Keywords: Multiscale modeling; Molecular dynamics; Computational chemistry; Nanotechnology; Polymers

* Corresponding Author, Tel.: (906) 487-2329; fax: (906) 487-2822; E-mail address: gmodegar@mtu.edu

1. Introduction

Polymers and polymer nanocomposites are important materials in the design of aerospace structures because of their large stiffness-to-weight and strength-to-weight ratios relative to metal- and ceramic-based materials. To facilitate the development of these materials, multiscale modeling strategies must be developed that predict the bulk mechanical properties of the materials as a function of the molecular structure.

Molecular Mechanics (MM) and Molecular Dynamics (MD) simulation techniques can be used to predict the molecular structure of a material and the behavior of the molecular systems when subjected to applied mechanical deformations. Many studies have focused on modeling and simulation of polymers and polymer-based nanocomposites via MM and MD techniques (Theodorou and Suter, 1986; Fan et al., 1994; Lordi and Yao, 2000; Sane et al., 2002; Frankland et al., 2003; Griebel and Hamaekers, 2004; Hu and Sinnott, 2004; Liang et al., 2004; Odegard et al., 2004; Odegard et al., 2005; Shenogin and Ozisik, 2005). These studies have demonstrated that molecular modeling techniques can be effectively used to predict both structure and elastic mechanical properties of polymer-based material systems. Three important factors required for the accurate prediction of properties of polymer material systems using a multiscale modeling approach are: (1) the assumed continuum mechanics-based constitutive relationship, (2) the selection of the molecular-level interatomic potential, and (3) the molecular modeling procedure.

To accurately describe the mechanical stress-strain response of polymer-based materials subjected to large deformations, it is necessary to formulate the constitutive law within a finite-deformation framework. While hyperelastic formulations have been developed and characterized for compressible and incompressible materials (Ogden, 1997; Holzapfel, 2000), they have been scarcely used in the multiscale modeling of polymer-based materials. It is proposed that formulation of hyperelastic constitutive equations, in conjunction with molecular modeling, can be used for the development of reliable structure-property relationships in polymer material systems.

Several simplified atomic potentials, or force fields, for organic-based material systems have been developed in recent years that describe the interactions between bonded and non-bonded atoms (Brooks et al., 1983; Allinger et al., 1989; Clark et al., 1989; Cornell et al., 1995; Jorgensen et al., 1996; Ott and Meyer, 1996; Sun, 1998). Each of these force fields has been characterized via experimental techniques and quantum computations and is described by their own set of unique parameters and functional forms. Even though it is expected that these different parameters and forms will affect the relationship between force field type and predicted mechanical properties, little is known about the specific cause-and-effect relationships as applied to polymeric materials.

The establishment of a molecular structure for a polymer material before and after deformation, for a given force field, can be achieved with either static or dynamic molecular simulation techniques using MM and MD, respectively. With the static approach, the potential energy of the molecular system, as defined by the force field, is minimized to reach the equilibrated state. While the static procedure converges onto the equilibrated structure quickly, the mapping of real time molecular motion onto the molecular structure is lost. With the dynamic approach, the

motion of the individual atoms in real time is determined using Newton's laws of motion. While the dynamic approach preserves time as the independent variable with the corresponding molecular structure, convergence onto a minimized molecular energy can be computationally more time-intensive than with the static approach. It is unclear how these different approaches affect the accurate prediction of mechanical properties of polymer-based materials using a multiscale approach.

Therefore, the objective of the present paper is to develop a multiscale modeling technique based on molecular simulations and hyperelasticity to predict elastic constitutive properties of two different polymer systems. The predicted values of elastic properties, unique for each combination of force field and modeling technique, will be compared to experimentally-measured values. The polymers include a polycarbonate (Figure 1) and a polyimide from 3,3',4,4'-biphenyltetracarboxylic dianhydride (BPDA) and 1,3-bis(4-aminophenoxy)benzene (APB) monomers (Figure 2) (Srinivas et al., 1997; Hergenrother et al., 2002). The three force fields used in this study are described in subsequent sections of the paper. Based on the comparison of prediction to experiment, the most appropriate force field and modeling technique for the prediction of mechanical properties of polymer-based nanocomposite systems is determined.

2. Force Fields

Three distinct force fields were used in this study to simulate the polymer deformations and provide inputs necessary to compute the mechanical properties; AMBER (Cornell et al., 1995) (without electrostatic interactions), OPLS-AA (Jorgensen et al., 1996; Kaminsky et al., 2001), and MM3 (Allinger et al., 1989). Each of the force fields has a unique functional form and set of force constants, which is summarized in the Appendix. These three force fields were chosen because of their frequent use in computational chemistry research and because of their flexibility in modeling a wide range of atom and bonding types. Other popular atomic potentials include the Brenner (Brenner, 1990) and Tersoff (Tersoff, 1988, 1988) potentials. The Tersoff potential was primarily developed for the modeling of silicon systems, and was later extended to accommodate graphite and amorphous carbon systems. The Brenner potential is a highly parameterized version of Tersoff's formalism. Because the Brenner and Tersoff potentials are restricted to hydrocarbon and silicon systems and many polymers contain more than just carbon, hydrogen, or silicon atoms, the Brenner and Tersoff potentials were not used in the present study.

Each of the force constants for these three force fields is unique for each force field and interacting atom types. For all three force fields, it was assumed that torsional force constants that were not defined in the respective literature references or by the simulation software (Ponder, 2004) were zero-valued. For the AMBER force field, the specific force constants used were those specified by the AMBER99 parameter set in the simulation software.

3. Equivalent-Continuum Modeling

The nonlinear-elastic (hyperelastic) properties of the two material systems were determined using the Equivalent-Continuum Modeling method (Odegard et al., 2002; Odegard et al., 2003; Odegard et al., 2005; Odegard et al., 2005). This modeling technique is ideally suited for large,

amorphous atomic structures with a mixture of covalent and secondary chemical bonds, as the Cauchy-Born rule is ignored because of immense computational complexity that would result if it was incorporated under these conditions. It is important to note that the nonlinearity in the constitutive modeling referrers only to the hyperelastic approach incorporated, not the presence of constitutive nonlinearities, such as plasticity. This approach consisted of three steps. First, representative volume elements (RVEs) of the molecular structures of both polymers for each force field were chosen that accurately described the bulk structures of the materials. Next, a constitutive law that described the behavior of the equivalent-continuum model was established. Finally, the energies of deformation of the two models were equated under identical sets of boundary conditions to determine each of the material parameters in the constitutive equation. Each of these steps is described in detail below.

3.1. Representative Volume Element

The RVEs of the molecular models were established from the equilibrium molecular structures of the polymers for each force field determined using MD simulations. The molecular structures of the polymers represent the room temperature condition. The RVE geometry of the molecular models selected was a cubic box and the specific configuration for the two polymer systems were established as described below.

The polycarbonate model was initially prepared in the gas phase. Six chains of 20 monomer units each (a total of 3972 atoms) were constructed and the system was condensed to a low density with an NPT (constant number of atoms, pressure, and temperature) MD simulation at 300K and 1 atm for 50 ps. This process was followed by an NVT (constant number of atoms, volume, and temperature) simulation for 100 ps at 600K. The temperature was reduced in a stepwise fashion with a series of NPT MD simulations at 1 atm pressure to obtain the final equilibrated system. These equilibration simulations were performed with the CVFF force field (Dauber-Osguthorpe et al., 1988).

The molecular model of the polyimide was prepared with the aid of a reverse-mapping procedure that utilizes a coarse-grained model (Clancy, 2004). In this process, each polyimide molecule, in the coarse-grained structure was a linked vector model used to represent the rigid rings that comprise the polyimide backbone (Figure 3). The linked vectors followed the contour of the molecule. The parameters used for this model consisted of angular distributions between consecutive vectors and long-range forces between beads placed along the midpoint of each vector. These parameters were estimated from MD simulation of the polyimide monomers with the CVFF force field (Dauber-Osguthorpe et al., 1988). The centroids of the beads placed at the midpoint of each vector were the centers for interaction forces between non-adjacent beads along the chain of the polymer and between beads on different chains. The coarse-grained polymers were initially placed as random walk chains inside a simulation box such that the density was close to the bulk value. The bulk polymer model consisted of seven chains of polymers each composed of ten of the repeat units shown in Figure 2. The choice of seven chains was made to create a moderately large simulation box with 4214 atoms. In this initial placement, only the angular distributions between adjacent vectors along the chain were considered in the equilibration. Monte Carlo simulation was used to equilibrate the chains from their initial starting configuration. The simulation ran at 650K until relaxation of an autocorrelation

function (Leach, 2001) of the end vectors was achieved and the average centers of mass were displaced a distance greater than the square of the average radii of gyration. After sufficient equilibration with the coarse-grained Monte Carlo model, the chains were reverse-mapped to the fully atomistic configuration by replacing the deleted atoms back into position along the vectors of the coarse-grained model.

The resulting equilibrated atomistic structures for both polymers were subsequently subjected to NPT MD simulations for 200 ps at 300 K and 1 atm using the AMBER, OPLS-AA, and MM3 force fields respectively. These constant-pressure MD simulations allowed the atomistic structures to relax to the equilibrium density and thus any residual stresses averaged over the RVE were minimized. It was assumed that this step also eliminated any spurious effects of using different techniques to create the two polymer structures. The employed algorithm preserved the cubic structure of the simulation box while allowing the size of the simulation box to change. The final periodic boundary box sizes varied from 37.7 Å to 47.2 Å on a side depending on the force field used. After the NPT MD simulations, the densities of the polycarbonate were 1.2, 0.4, and 1.1 g/cm^3 for the AMBER, OPLS-AA, and MM3 force fields, respectively, and the densities of the polyimide were 1.0, 0.6, and 1.2 g/cm^3 for the AMBER, OPLS-AA, and MM3 force fields, respectively. The densities for the two polymers predicted with the AMBER and MM3 force fields are within the range of reasonable values of 1.2 - 1.4 g/cm^3 (Ashby and Jones, 1996). However, the densities of the polymers predicted with the OPLS-AA force field are much lower than the expected values. Examples of RVEs of the polycarbonate and polyimide are shown in Figures 4 and 5, respectively.

3.2. Constitutive Equation

For the computational simulation of a hyperelastic polymer material subjected to finite deformation, it is assumed that the strain-energy function is associated with stress and deformation tensors that are thermodynamic work conjugates in the balance of mechanical energy and satisfies the Clausius-Duhem inequality and the requirement of observer-frame indifference (known as the hyperelastic approach) (Truesdell and Noll, 2004). Although many authors choose to model the deformation of polymers using a strain-energy function based on a free energy associated with changes in entropy (known as the statistical approach) (Flory, 1953), it has been shown that the hyperelastic approach yields more accurate results than the statistical approach (Ogden, 1997). Furthermore, the statistical approach neglects all molecular interactions except the straightening of the polymer chains, while the hyperelastic approach can consider a wide range of polymer degrees of freedom, such as those specified in Equations (A.1) - (A.18).

The second Piola-Kirchhoff stress tensor is

$$\mathbf{S} = 2\frac{\partial \Psi_c(\mathbf{C})}{\partial \mathbf{C}} \tag{1}$$

where $\mathbf{C}$ is the right Cauchy-Green deformation tensor and Ψ_c is the scalar strain-energy density function of the equivalent continuum. The second Piola-Kirchhoff stress tensor and the right

Cauchy-Green deformation tensor are henceforth referred to as the stress tensor and deformation tensors, respectively. The deformation tensor is defined as

$$\mathbf{C} = \mathbf{F}^T\mathbf{F} \tag{2}$$

where **F** is the deformation gradient tensor whose components are given by

$$F_{ij} = \frac{\partial x_i}{\partial X_j} \tag{3}$$

In Equation (3), the vector components X_i and x_i are the material (undeformed) and the spatial (deformed) coordinates, respectively, which are related by the deformation equations (Ogden, 1997)

$$\mathbf{x} = \chi(\mathbf{X}, t) \tag{4}$$

where t is time. The ratio of the deformed to the undeformed volume is given by the Jacobian, J, which is defined as the determinate of the deformation gradient tensor.

All polymers, in general, are viscoelastic and experience time-dependent behavior. However, because of the time-scale limitations in the atomistic modeling of polymers, it is assumed in this study that the polymers exhibit a hyperelastic, time-independent response. This assumption does not preclude the use of time-dependent models for the mechanical behavior of polymers (Drozdov, 1996; Holzapfel, 2000). Therefore, Equation (4) reduces to

$$\mathbf{x} = \chi(\mathbf{X}) \tag{5}$$

The functional form of the strain-energy density is restricted by considering the invariance properties of the material such that the strain-energy density remains invariant with respect to the coordinate transformations expressed by the material symmetry. For an isotropic material, the reducible invariants of the deformation tensor **C** are

$$\begin{aligned} I_1 &= \mathrm{tr}(\mathbf{C}) \\ I_2 &= \frac{1}{2}\left\{\left[\mathrm{tr}(\mathbf{C})\right]^2 - \mathrm{tr}(\mathbf{C}^2)\right\} \\ I_3 &= \det(\mathbf{C}) \end{aligned} \tag{6}$$

where tr(**C**) and det(**C**) are the trace and determinate of tensor **C**, respectively. In addition to the symmetry requirement, the functional form of the strain-energy density function must also satisfy the global existence requirement of polyconvexity (Ball, 1977). While the physical meaning of polyconvexity is not well-understood, the extensive mathematical details of polyconvex strain-energy density function formulation can be found elsewhere (Ball, 1977; Ciarlet, 1988; Marsden and Hughes, 1994). It is clear that the strain-energy density function can be expressed as a linear combination of scalar invariant functions of I_1, I_2, and I_3; each of which

satisfies convexity. Therefore, a strain-energy density function that satisfies this requirement has the form

$$\Psi_c = \sum_{k=1}^{n} \psi_k \left(I_1, I_2, I_3 \right) \tag{7}$$

where ψ_k are n convex scalar functions. Using the chain rule of calculus, Equation (1) becomes

$$\mathbf{S} = 2\sum_{k=1}^{n} \frac{\partial \psi_k \left(I_1, I_2, I_3 \right)}{\partial \mathbf{C}} = 2\sum_{k=1}^{n} \left(\frac{\partial \psi_n}{\partial I_1} \frac{\partial I_1}{\partial \mathbf{C}} + \frac{\partial \psi_n}{\partial I_2} \frac{\partial I_2}{\partial \mathbf{C}} + \frac{\partial \psi_n}{\partial I_3} \frac{\partial I_3}{\partial \mathbf{C}} \right) \tag{8}$$

It can be shown that

$$\begin{aligned} \frac{\partial I_1}{\partial \mathbf{C}} &= \mathbf{I} \\ \frac{\partial I_2}{\partial \mathbf{C}} &= I_1 \mathbf{I} - \mathbf{C} \\ \frac{\partial I_3}{\partial \mathbf{C}} &= I_3 \mathbf{C}^{-1} \end{aligned} \tag{9}$$

A set of convex functions for ψ_k are (Schroder and Neff, 2003)

$$\psi_1 = c_1 \left(I_3 - 1 \right)^2 \tag{10}$$

$$\psi_2 = c_2 \left(\frac{I_1}{I_3^{1/3}} - 3 \right) \tag{11}$$

$$\psi_3 = c_3 \left(\frac{I_2^{\,3}}{I_3^{\,2}} - 27 \right) \tag{12}$$

where c_1, c_2, and c_3 are material constants and c_1, c_2, $c_3 \geq 0$. It has been shown (Schroder and Neff, 2003) that Equation (10) corresponds to the purely volumetric portion of the total material deformation, while Equations (11) and (12) correspond to the isochoric, or volume preserving, portion of the total deformation. Because Equations (11) and (12) both correspond to isochoric deformation, these terms can be combined such that $c_2 = c_3$, and the total strain-energy density from Equations (7) and (10)-(12) is

$$\Psi_c = \psi_1 + \psi_2 + \psi_3 = \psi_{\text{vol}} + \psi_{\text{iso}} = c_1 \left(I_3 - 1 \right)^2 + c_2 \left(\frac{I_1}{I_3^{1/3}} + \frac{I_2^{\,3}}{I_3^{\,2}} - 30 \right) \tag{13}$$

where ψ_{vol} and ψ_{iso} are the strain energy densities associated with volumetric and isochoric deformations, respectively. Equation (13) can be rewritten as

$$\Psi_c = c_1\Omega_1 + c_2\Omega_2 \tag{14}$$

where

$$\begin{aligned}\Omega_1 &= \left(I_3 - 1\right)^2 \\ \Omega_2 &= \left(\frac{I_1}{I_3^{1/3}} + \frac{I_2^{\,3}}{I_3^{\,2}} - 30\right)\end{aligned} \tag{15}$$

The quantities Ω_1 and Ω_2 are introduced to denote the volumetric and isochoric deformation terms, respectively, independent of the material parameters c_1 and c_2. Substitution of Equation (13) into (8) yields

$$\mathbf{S} = \frac{2}{3}\left[6c_1 I_3\left(I_3 - 1\right) - c_2\left(\frac{I_1}{I_3^{1/3}} + 6\frac{I_2^{\,3}}{I_3^{\,2}}\right)\right]\mathbf{C}^{-1} + 2c_2\left(\frac{1}{I_3^{1/3}} + 3\frac{I_1 I_2^{\,2}}{I_3^{\,2}}\right)\mathbf{I} - 6c_2\frac{I_2^{\,2}}{I_3^{\,2}}\mathbf{C} \tag{16}$$

Equation (13) satisfies the normalization condition, that is, it vanishes in the undeformed configuration

$$\Psi_c\left(I_1 = 3, I_2 = 3, I_3 = 1\right) = 0 \tag{17}$$

Equation (13) also satisfies the required growth conditions. Specifically, as the Jacobian approaches zero (vanishing volume), and as the Jacobian approaches infinity (infinite deformation), the strain-energy density approaches infinity,

$$\lim_{\det\mathbf{F}\to 0} \Psi_c = \infty \tag{18}$$

$$\lim_{\det\mathbf{F}\to \infty} \Psi_c = \infty \tag{19}$$

Equation (16) describes the mechanical behavior of the equivalent-continuum model. At this point, however, the materials constants c_1 and c_2 are unknown, and must be determined using the molecular structure of the polymer. This is accomplished in the subsequent modeling step.

3.3. Energy Equivalence

The energies of deformation of the equivalent-continuum, Ψ_c, and molecular models, Ψ_m, were equated for identical sets of boundary conditions to determine the bulk mechanical properties of the polyimide for each of the force fields. The molecular strain-energy density (potential energy) is

$$\Psi_m = \frac{1}{V_0}\left(\Lambda_{total} - \Lambda_{total}^0\right) = \frac{\Delta\Lambda}{V_0} \tag{20}$$

where Λ_{total}^{0} and Λ_{total} are the potential energies of the molecular model from either Equations (A.1), (A.6), or (A.11) before and after deformation, respectively, and V_0 is the initial volume of the RVE. For finite deformations, the deformation of the boundary of the RVE is generalized by Equation (5).

Because the strain-energy density of the equivalent continuum, Ψ_c, is the sum of the volumetric and isochoric deformation components, as shown in Equations (13) - (15), volumetric and isochoric modes of deformation were applied to the molecular models to determine the material parameters c_1 and c_2. For each deformation, the strain-energy densities in Equations (14) and (20) were equated by adjusting these two material parameters. To relate these deformations to those typically applied to a specimen during laboratory testing, the deformation levels are expressed in terms of the Lagrangian strain tensor (henceforth referred to as the strain tensor)

$$\mathbf{E} = \frac{1}{2}\left(\mathbf{C} - \mathbf{I}\right) \tag{21}$$

For the volumetric deformations, the deformation equations are

$$\mathbf{x}^{(k)} = \alpha_k \mathbf{x}^{(k-1)} \tag{22}$$

where the deformation step k = 1, 2, 3, 4; $\mathbf{x}^{(0)} = \mathbf{X}$; and α_k is the scalar constant corresponding to the k^{th} deformation step. The spatial coordinates $\mathbf{x}^{(1)}$, $\mathbf{x}^{(2)}$, $\mathbf{x}^{(3)}$, and $\mathbf{x}^{(4)}$ correspond to volumetric strains ($E_{11} = E_{22} = E_{33}$) of 0.25%, 0.50%, 0.75%, and 1.0%, respectively. The relative deformation gradient tensor components, which relate the deformation at a given strain level to those of the previous strain level are

$$F'_{ij}\left(\mathbf{x}^{(k)}\right) = \frac{\partial x_i^{(k)}}{\partial x_j^{(k-1)}} \tag{23}$$

where $\mathbf{F}'\left(x^{(1)}\right) = \mathbf{F}\left(x^{(1)}\right)$. Therefore, the deformation gradient tensor components that relate the coordinate for each strain level to those of the material coordinate system are

$$F_{ij}\left(\mathbf{x}^{(k)}\right) = \frac{\partial x_i^{(k)}}{\partial X_j} = F'_{im}\left(\mathbf{x}^{(k)}\right) F_{mj}\left(\mathbf{x}^{(k-1)}\right) \tag{24}$$

where $\mathbf{F}(\mathbf{x}^{(0)}) = \mathbf{I}$. Using Equations (21) - (24), the constants α_1, α_2, α_3, and α_4 where adjusted to achieve the exact desired volumetric strain levels in Equation (21). These values are listed in Table I.

The deformation equations for the isochoric deformations are

$$\begin{aligned} x_1^{(1)} &= \beta_1 \left(X_2 + X_3 \right) + X_1 \\ x_2^{(1)} &= \beta_1 \left(X_1 + X_3 \right) + X_2 \\ x_3^{(1)} &= \beta_1 \left(X_1 + X_2 \right) + X_3 \\ x_1^{(k)} &= \beta_k \left(x_2^{(k-1)} + x_3^{(k-1)} \right) + x_1^{(k-1)} \\ x_2^{(k)} &= \beta_k \left(x_1^{(k-1)} + x_3^{(k-1)} \right) + x_2^{(k-1)} \\ x_3^{(k)} &= \beta_k \left(x_1^{(k-1)} + x_2^{(k-1)} \right) + x_3^{(k-1)} \end{aligned} \tag{25}$$

where β_1, β_2, β_3, and β_4 are scalar constants and the superscripts 1, 2, 3, and 4 (k = 2, 3, and 4) correspond to 3-dimensional shear strain levels of $\gamma_{23} = \gamma_{13} = \gamma_{12}$ = 0.25%, 0.50%, 0.75%, and 1.0%, respectively ($\gamma_{ij} = 2E_{ij}$ when $i \neq j$). Similar to the case of the volumetric deformation, the constants β_1, β_2, β_3, and β_4 were adjusted such that these shear strains were achieved by using Equations (21) and (23) - (25). The values of the β constants are listed in Table I.

The change in the potential energies of the molecular models, $\Delta\Lambda$ in Equation (20), were determined using static (MM) and dynamic (MD) molecular simulations. Both volumetric and isochoric deformations were applied to the equilibrium molecular structures for each force field by deforming the RVE and all of the atoms in the models according to the applied deformation field. In the static simulations, an energy minimization technique was subsequently performed using a quasi-Newton L-BFGS method (Nocedal and Wright, 1999) as implemented with the MINIMIZE program in the TINKER modeling package (Ponder, 2004). The minimizations were executed for RMS gradient values of of 0.1 kcal/mole/Å. During the energy minimization, the RVE volume was kept constant as the atoms were shifted to minimize the potential energy. In the dynamical simulations, an NVT simulation with periodic boundary conditions was subsequently used for each deformation to allow the RVE dimensions to remain fixed while the atoms were allowed to move into new equilibrium positions. The dynamic molecular simulations were run up to 40 ps with 1.0 fs time steps at 298 K, and were performed using the TINKER modeling package (Ponder, 2004). The potential energies of deformation of the molecular models were averaged over the final 10 ps of each simulation, as for the first 30 ps showed significant changes in the potential energy as the molecular structure relaxed into the deformed configuration. The temperatures of the simulations were monitored with the Groningen method of coupling to an external bath (Berendsen et al., 1984). The temperature of the system was achieved through modification of the equation of motion by the use of stochastic and friction terms yielding a Langevin equation. As a result of this modification in the equation of motion, the velocities were scaled to achieve the desired temperature of the system. The simulations were repeated for all necessary deformation modes of each polymer. Therefore, a total of nine (including the undeformed configuration) strain-energy densities of the molecular model, Ψ_m, were determined for the complete range of deformations. For the static simulations, the repeated values of Ψ_m were identical to the original set.

For the static and dynamic simulations, periodic boundary conditions were applied such that atoms were free to cross the boundary of the deformed and undeformed simulation cells. Atoms that crossed the boundary entered the simulation cells on the opposite side, as described in detail elsewhere (Leach, 2001). Therefore, none of the atoms in the molecular simulations were kinematically over-constrained, as can occur in simulations of RVEs of heterogeneous material systems with kinematic boundary conditions (Sun and Vaidya, 1996; Jiang et al., 2002).

4. Results and Discussion

Because Equation (14) is linear in Ω_1 and Ω_2, the strain-energy density of the molecular models is plotted with respect to Ω_1 and Ω_2 in Figures 6 and 7, respectively, for the static molecular simulations. From Figures 6 and 7 it is evident there is a slight nonlinearity in the data. Ideally, for materials under large elastic deformations, the slope of the curves in Figures 6 and 7 would be expected to be linear, as indicated by Equation (14). Therefore, for larger deformations in the static simulations, a small amount strain-energy density is lost, most likely because of viscoelastic relaxation of the polymer chains or because of an evolution of damage on the molecular level (e.g. void nucleation). Because of the difficulty in quantifying the simulated time in static molecular simulations, viscoelastic relaxation can be neither verified nor characterized for this data.

Similarly, the molecular strain-energy densities for the volumetric and isochoric deformations are shown in Figures 8 and 9, respectively, from the dynamic simulations. Specific trends in the plotted data are difficult to discern due to the scatter for each loading level, force field, and polymer. This scatter is mostly a result of the motions (velocities) of the atoms and the resulting fluctuations in atomic coordinates and pressure for each simulation time step (Leach, 2001). It is expected that as the number of atoms in the simulation RVEs increase, this scatter will decrease. That is, as the number of vibrating atoms in the simulation cell increases, each with its own velocity components at a give time step, the overall fluctuation of the energy will decrease. Of course, at the bulk level, such arbitrary fluctuations in energy are not witnessed because of the large number of total atoms that are being observed in an element of material. Because of the existence of the data scatter in Figures 8 and 9, the nonlinear behavior observed in the static simulations is not observed in the dynamic simulations.

From Figures 6 - 9, it is evident that the slopes of each set of data do not necessarily approach a molecular potential energy value of zero as Ω_1 and Ω_2 approach zero. In the establishment of material RVEs using finite-sized molecular systems, as described section 3.1, it is very difficult to obtain a completely stress-free system in the reference configuration using an NPT simulation. This is because of the unavoidable, small fluctuations of the pressure in NPT simulations (even though the pressure changes are minimized) (Leach, 2001). Therefore, the RVEs for each material and force field are not completely free of residual stresses.

For both static and dynamic simulations, linear least-squares regressions were performed for the Ψ_m vs. Ω_1 and Ω_2 data sets shown in Figures 6 - 9 for each loading condition, polymer, and force field. Because Equation (14) is linear in Ω_1 and Ω_2, the slopes of the regression curves in Figures 6 and 8 are the material parameter c_1, and the slopes of the regression curves in Figures 7 and 9 are the material parameter c_2. Because of the aforementioned residual stress in the

molecular modeling data, the linear regressions were performed over the deformation increments without forcing the regression to approach a zero-valued molecular potential energy as Ω_1 and Ω_2 approached zero. Therefore, the slopes of the regressions accurately reflect the values of c_1 and c_2 in a bulk-level material without the existence of any residual stresses. The values of the material parameters c_1 and c_2 are listed in Tables II and III for the static and dynamic simulations, respectively.

The constitutive relationship in Equation (16) and the material parameters in Tables II and III were used to predict the stress-strain responses of the two polymer systems. Figures 10 and 11 depict the hydrostatic stress-volumetric strain curves using the parameters from the static and dynamic simulations, respectively. For this loading condition, it was assumed that $C_{11} = C_{22} = C_{33}$ with all other C_{ij} equal to zero. The volumetric strain was

$$\frac{\Delta V}{V} = 3E_{11} = 3E_{22} = 3E_{33} \tag{26}$$

The corresponding hydrostatic stress was given by Equation (16) where $S_{11} = S_{22} = S_{33}$ with all other S_{ij} equal to zero. In Figures 10 and 11, the mechanical responses of both polymers are linear, as expected, and their slopes are the bulk moduli as predicted by the constitutive law and the material parameters. Figures 12 and 13 illustrate the shear stress-shear strain (S_{12} versus γ_{12}) response of the two polymers from Equation (16) using the static and dynamic simulations parameters, respectively, in Tables II and III. For this loading condition, it was assumed that $C_{11} = C_{22} = C_{33} = 1$, $C_{23} = C_{13} = 0$, and $C_{12} \neq 0$. The resulting stress state was $S_{12} \neq 0$ with all other $S_{ij} = 0$. Because the responses of the two polymer systems in both figures are linear over the given range of shear strains, the slope of the curves is the predicted shear modulus. The Young's and shear moduli of the two polymer systems for the three force fields and two simulation types, listed in Tables IV and V, were determined from the data shown in Figures 10-13 and from the standard relations for elastic properties of isotropic materials (Malvern, 1969). Experimentally-determined values of the Young's and shear moduli for the polycarbonate (Christopher and Fox, 1962) and the polyimide, with an assumed Poisson's ratio of 0.4 (Hergenrother et al., 2002), are also listed in Tables IV and V, respectively. The data in Figures 10 – 13 were plotted for relatively small deformations because the data for larger deformations shows the same trends and the modeling procedure does not model larger deformation effects such as plastic yielding or craze formation.

From the data in Tables IV and V, the static simulations predicted mechanical properties that are lower than those predicted by the dynamic simulations for both polymer materials. Comparison of the properties from static and dynamic simulations also reveals that the properties predicted with the static simulations are closer to the experimentally-obtained values. For the properties predicted from static simulations, the OPLS-AA and MM3 force fields predicted mechanical properties that are lower than those predicted with the AMBER force field. Also, the static simulations predict Young's and shear moduli that are higher than those from experiment with the AMBER force field, while the same predicted properties are lower than the experiment with the OPLS-AA and MM3 force fields. There are no distinct trends between predicted moduli and polymer type or force field for the dynamic simulations.

5. Summary and Conclusions

In this study, a combined atomistic-hyperelastic multiscale modeling technique, based on the Equivalent-Continuum Model, was developed and used to predict elastic properties of polycarbonate and polyimide polymer systems using the AMBER, OPLS-AA, and MM3 molecular force fields. The hyperelastic model was formulated with a strain-energy potential function that had a functional form based on molecular simulation predictions. Both static and dynamic molecular simulations were performed using Molecular Mechanics and Molecular Dynamics simulation techniques, respectively. The predicted bulk properties of the polymers using the three force fields were compared to experimentally-measured values.

5.1. Static versus Dynamic Simulation

Examination of the predicted values of Young's and shear moduli for the two polymers indicates that the static simulations predicted mechanical properties that are lower than those predicted by the dynamic simulations, with the properties from static simulations closer to the experimental properties than the properties from the dynamic simulations. These results can be attributed to two possible factors, data scatter and mechanical relaxation.

The results indicate that the scatter in the data from the dynamic simulations is much greater than that from the static simulations and therefore there is a greater chance of the dynamic simulations yielding predicted mechanical properties that are less accurate than those from the static simulations (when comparing to the experiment). It is expected that with dynamic simulations of larger molecular systems, the scatter would generally decrease.

The mechanical relaxation of the polymer chains that occurs in the experiments and in the static simulations is not expected to be accurately accounted for in the dynamic simulations. Polymers generally behave in a viscoelastic manner when subjected to applied deformations because of the time-dependent response of polymer-chain sliding and chain-torsional motions. Therefore, in the experiments, it is speculated that the strain rates were small enough that mechanical relaxation occurred as the specimens were deformed, thus reducing the resultant stress on the specimen. In the static simulations, energy minimizations are performed that mimic the relaxation mechanisms of a deformed polymer; conversely, in the dynamic simulations, the time scale is on the order of picoseconds, which is not long enough to allow for significant mechanical relaxation. Therefore, the strain-energy density is much higher for a given deformation in the dynamic simulations relative to the static simulations, and the corresponding constitutive equations will predict higher stresses for a given applied deformation. As a result, the predicted elastic material properties from the dynamic simulations are greater than those from the static simulations and the experiments.

5.2. Force Field Comparisons

The predicted moduli from the static simulations are larger than those from experiment for the AMBER force field, and are smaller than the experimental values for the OPLS-AA and MM3 force fields. The relatively low predicted elastic properties from the OPLS-AA force field are likely a direct result of the lower simulated polymer densities because it is expected that higher

elastic constants would result from simulations of denser materials. The functional forms of the AMBER and OPLS-AA force fields, from Equations (A.1) to (A.10), are nearly identical. The differences in the two force fields (as used in this study) are the presence of electrostatic interactions in the OPLS-AA force field and the differences in the force constant parameters, particularly for the torsions. These differences result in the significantly different predicted densities for both polymer systems. The lower predicted properties of the MM3 static simulations cannot be attributed to the same effect because the simulated material densities were close to the expected values. The functional form of the MM3 force field from Equations (A.11) - (A.18) attempts to account for a wider range of behavior than those of the AMBER and OPLS-AA force fields. However, because the predicted properties using the MM3 force field in static simulations are farther from the experimental properties than those predicted with the AMBER and OPLS-AA force fields, the more complex functional form does not predict properties as accurately as the more simple functional forms of AMBER and OPLS-AA for the polymer systems used in this study.

The relatively high predicted mechanical properties from the static simulations with the AMBER force field follow a trend that has been observed in the literature. Previous studies (Fan and Hsu, 1992; Fan et al., 1994) have pointed out that the predicted mechanical properties from molecular simulations are expected to be 50 - 100% larger than those obtained from experiments. In the current study, the predicted properties from the AMBER force field were 70 - 115% higher than experiment. Most likely, this difference can be attributed to the fact that the RVEs in molecular modeling simulations represent a nearly perfect molecular structure, whereas, in the actual experimental test specimens, the material contains low volume fractions of air pockets, inclusions, and unreacted monomers. Therefore, it is expected that simulated mechanical properties should be larger than experimentally-obtained properties if the polymer system imperfections are not included in the molecular modeling. It is also expected that the computational modeling of these imperfections in these polymer systems would yield predicted properties that are closer to the experiment than those predicted in the current study. From this perspective, for the polymer systems investigated in this study, the AMBER force field appears to be more accurate than the OPLS-AA and MM3 force fields for predicting elastic properties.

Acknowledgements

This research was sponsored by NASA Langley Research Center under grant NNL04AA85G and under the NASA cooperative agreement NCC-1-02043 with the National Institute of Aerospace.

Appendix

The total potential energy of a simulated molecular system computed with the AMBER force field is based on the summation of the bond stretching, bending, torsion and nonbonded energies given by

$$\Lambda^{A}_{\text{total}} = \Lambda^{A}_{\text{stretch}} + \Lambda^{A}_{\text{bend}} + \Lambda^{A}_{\text{torsion}} + \Lambda^{A}_{\text{nb}} \tag{A.1}$$

where superscript *A* indicates the AMBER force field and

$$\Lambda^A_{\text{stretch}} = \sum_{\text{stretch}} K^A_r \left(r - r^A_{eq}\right)^2 \tag{A.2}$$

$$\Lambda^A_{\text{bend}} = \sum_{\text{bend}} K^A_\theta \left(\theta - \theta^A_{eq}\right)^2 \tag{A.3}$$

$$\Lambda^A_{\text{torsion}} = \sum_{\text{torsion}} \left\{ \frac{V^A_1}{2}\left[1+\cos\left(\phi+\zeta^A\right)\right] + \frac{V^A_2}{2}\left[1-\cos\left(2\phi+\zeta^A\right)\right] + \frac{V^A_3}{2}\left[1+\cos\left(3\phi+\zeta^A\right)\right] \right\} \tag{A.4}$$

$$\Lambda^A_{\text{nb}} = \sum_{I<J} 4\varepsilon^A_{IJ}\left[\frac{\left(\sigma^A_{IJ}\right)^{12}}{r_{IJ}{}^{12}} - \frac{\left(\sigma^A_{IJ}\right)^{6}}{r_{IJ}{}^{6}} \right] \tag{A.5}$$

where the summations are taken over all of the corresponding interactions in the molecular model; K^A_r and K^A_θ are the bond-stretching and bond-angle bending force constants, respectively; r and r^A_{eq} are the bond length and equilibrium bond length, respectively; θ and θ^A_{eq} are the bond angle and equilibrium bond angle, respectively; $V^A_n/2$, ζ^A, and ϕ are the torsion magnitude (n=1,2,3), phase offset, and the torsion angle, respectively; and ε^A_{IJ}, r_{IJ}, and σ^A_{IJ} are van der Waals well depth, non-bonded distance between atoms I and J, and the equilibrium distance between atoms I and J, respectively.

Similarly, the total potential energy of the molecular model computed with the OPLS-AA force field is generally represented by

$$\Lambda^O_{\text{total}} = \Lambda^O_{\text{stretch}} + \Lambda^O_{\text{bend}} + \Lambda^O_{\text{torsion}} + \Lambda^O_{\text{nb}} \tag{A.6}$$

where the superscript O indicates the OPLS-AA force field and

$$\Lambda^O_{\text{stretch}} = \sum_{\text{stretch}} K^O_r \left(r - r^O_{eq}\right)^2 \tag{A.7}$$

$$\Lambda^O_{\text{bend}} = \sum_{\text{bend}} K^O_\theta \left(\theta - \theta^O_{eq}\right)^2 \tag{A.8}$$

$$\Lambda^O_{\text{torsion}} = \sum_{\text{torsion}} \left\{ \frac{V^O_1}{2}\left[1+\cos\left(\phi+\zeta^O\right)\right] + \frac{V^O_2}{2}\left[1-\cos\left(2\phi+\zeta^O\right)\right] + \frac{V^O_3}{2}\left[1+\cos\left(3\phi+\zeta^O\right)\right] \right\} \tag{A.9}$$

$$\Lambda^O_{\text{nb}} = \sum_{I<J} \left\{ \frac{q^O_I q^O_J \text{e}^2}{r_{IJ}} + 4\varepsilon^O_{IJ}\left[\frac{\left(\sigma^O_{IJ}\right)^{12}}{r_{IJ}{}^{12}} - \frac{\left(\sigma^O_{IJ}\right)^{6}}{r_{IJ}{}^{6}} \right] \right\} \tag{A.10}$$

where q_I is the partial charge of atom I, e is the elementary charge, and the remaining quantities are analogous to those already defined for the AMBER force field.

For the MM3 force field, the total potential energy includes the previously mentioned terms along with additional terms representing bond deformations given by stretch-bend, torsion-stretch, bend-bend, and the van-der-Walls and electrostatic interactions

$$\Lambda^M_{\text{total}} = \Lambda^M_{\text{stretch}} + \Lambda^M_{\text{bend}} + \Lambda^M_{\text{torsion}} + \Lambda^M_{\text{stretch-bend}} + \Lambda^M_{\text{torsion-stretch}} + \Lambda^M_{\text{bend-bend}} + \Lambda^M_{\text{vdw}} + \Lambda^M_{\text{electrostatic}} + \Lambda^M_{\text{nb}} \quad \text{(A.11)}$$

where the superscript *M* indicates the MM3 force field and

$$\Lambda^M_{\text{stretch}} = \sum_{\text{stretch}} 71.94 K_r^M \left(r - r_{eq}^M\right)^2 \left[1 - 2.55\left(r - r_{eq}^M\right) + 1.49\left(r - r_{eq}^M\right)^2\right] \quad \text{(A.12)}$$

$$\Lambda^M_{\text{bend}} = \sum_{\text{bend}} \left\{ \begin{array}{l} 0.021914 K_\theta^M \left(\theta - \theta_{eq}^M\right)^2 \times \\ \left[1 - 0.014\left(\theta - \theta_{eq}^M\right) + 5.6\left(10^{-5}\right)\left(\theta - \theta_{eq}^M\right)^2 \right. \\ \left. -7.0\left(10^{-7}\right)\left(\theta - \theta_{eq}^M\right)^3 + 9.0\left(10^{-10}\right)\left(\theta - \theta_{eq}^M\right)^4\right] \end{array} \right\} \quad \text{(A.13)}$$

$$\Lambda^M_{\text{torsion}} = \sum_{\text{torsion}} \left\{ \frac{V_1^M}{2}\left[1 + \cos\left(\phi\right)\right] + \frac{V_2^M}{2}\left[1 - \cos\left(2\phi\right)\right] + \frac{V_3^M}{2}\left[1 + \cos\left(3\phi\right)\right] \right\} \quad \text{(A.14)}$$

$$\Lambda^M_{\text{stretch-bend}} = \sum_{\text{stretch-bend}} 2.51118 K_{r\theta}^M \left[\left(r - r_{eq}^M\right) + \left(r' - r_{eq}^{\prime M}\right)\right]\left(\theta - \theta_{eq}^M\right) \quad \text{(A.15)}$$

$$\Lambda^M_{\text{torsion-stretch}} = \sum_{\text{torsion-stretch}} 11.995 \left(\frac{K_{\phi r}^M}{2}\right)\left(r - r_{eq}^M\right)\left[1 + \cos\left(3\phi\right)\right] \quad \text{(A.16)}$$

$$\Lambda^M_{\text{bend-bend}} = \sum_{\text{bend-bend}} \left[-0.021914 K_{\theta\theta'}^M \left(\theta - \theta_{eq}^M\right)\left(\theta' - \theta_{eq}^{\prime M}\right)\right] \quad \text{(A.17)}$$

$$\Lambda^M_{\text{vdw}} = \sum_{I<J} \varepsilon_{IJ}^M \left\{ -2.25\left[\frac{\left(\sigma_{IJ}^M\right)^6}{r_{IJ}^{\ 6}}\right] + 1.84\left(10^5\right)\exp\left[-12.00\left(\frac{\sigma_{IJ}^M}{r_{IJ}}\right)\right] \right\} \quad \text{(A.18)}$$

where $K_{r\theta}^M$, $K_{\phi r}^M$, and $K_{\theta\theta'}^M$ are force constants; r' and $r_{eq}^{\prime M}$ are the bond length and equilibrium bond length, respectively, of the adjacent covalent bond; and θ' and $\theta_{eq}^{\prime M}$ are the bond angle and equilibrium bond angle, respectively, of the adjacent bond angle. The energy contribution from electrostatic forces, $\Lambda^M_{\text{electrostatic}}$, is determined by either partial charges or dipole moments. The energies associated with all remaining non-bonded interactions, such as hydrogen bonding, are incorporated in Λ^M_{nb}. The remaining quantities in Equations (A.12)-(A.18) are analogous to those of the AMBER and OPLS-AA force fields.

References

Allinger, N.L., Yuh, Y.H. and Lii, J.H., 1989. Molecular Mechanics. The MM3 Force Field for Hydrocarbons. Journal of the American Chemical Society. 111, 8551-8566.

Ashby, M.F. and Jones, D.R.H., 1996. Engineering Materials 1: An Introduction to Their Properties & Applications. Butterworth-Heinemann, Oxford, UK.

Ball, J.M., 1977. Convexity Conditions and Existence Theorems in Nonlinear Elasticity. Archive for Rational Mechanics and Analysis. 63, 337-403.

Berendsen, H.J.C., Postma, J.P.M., van Gunsteren, W.F., DiNola, A. and Haak, J.R., 1984. Molecular Dynamics with Coupling to an External Bath. Journal of Chemical Physics. 81, 3684-3690.

Brenner, D.W., 1990. Empirical Potential for Hydrocarbons for use in Simulating the Chemical Vapor Deposition of Diamond Films. Physical Review B. 42, 9458-9471.

Brooks, F.P., Bruccoleri, R.E., Olafson, B.D., States, D.J., Swaminathan, S. and Karplus, M., 1983. CHARMM: A Program for Macomolecular Energy, Minimization, and Dynamics Calculations. Journal of Computational Chemistry. 4, 187-217.

Christopher, W.F. and Fox, D.W., 1962. Polycarbonates. Reinhold Publishing Corporation, New York.

Ciarlet, P.G., 1988. Mathematical Elasticity. Elsevier Science Publishers B.V., Amsterdam.

Clancy, T.C., 2004. Multi-Scale Modeling of Polyimides. Polymer. 45, 7001-7010.

Clark, M., Crammer, R.D. and Van Opdenhosch, N., 1989. Validation of the General Purpose Tripose 5.2 Force Field. Journal of Computational Chemistry. 10, 982-1012.

Cornell, W.D., Cieplak, P., Bayly, C.I., Gould, I.R., Merz, K.M., Ferguson, D.M., Spellmeyer, D.C., Fox, T., Caldwell, J.W. and Kollman, P.A., 1995. A Second Generation Force Field for the Simulation of Proteins, Nucleic Acids, and Organic Molecules. Journal of the American Chemical Society. 117, 5179-5197.

Dauber-Osguthorpe, P., Roberts, V.A., Osguthorpe, D.J., Wolff, J., Genest, M. and Hagler, A.T., 1988. Structure and Energetics of Ligand Binding to Protiens. Protiens: Structure, Function and Genetics. 4, 31-47.

Drozdov, A.D., 1996. Finite Elasticity and Viscoelasticity: A Course in the Nonlinear Mechanics of Solids. World Scientific, Singapore.

Fan, C.F., Cagin, T., Chen, Z.M. and Smith, K.A., 1994. Molecular Modeling of Polycarbonate. 1. Force Field, Static Structure, and Mechanical Properties. Macromolecules. 27, 2383-2391.

Fan, C.F. and Hsu, S.L., 1992. Application of the Molecular Simulation Technique to Characterize the Structure and Properties of an Aromatic Polysulfone System. 2. Mechanical and Thermal Properties. Macromolecules. 25, 266-270.

Flory, P.J., 1953. Principles of Polymer Chemistry. Cornell University Press, Ithaca, NY.

Frankland, S.J.V., Harik, V.M., Odegard, G.M., Brenner, D.W. and Gates, T.S., 2003. The Stress-Strain Behavior of Polymer-Nanotube Composites from Molecular Dynamics Simulation. Composites Science and Technology. 63, 1655-1661.

Griebel, M. and Hamaekers, J., 2004. Molecular Dynamics Simulations of the Elastic Moduli of Polymer-Carbon Nanotube Composites. Computer Methods in Applied Mechanics and Engineering. 193, 1773-1788.

Hergenrother, P.M., Watson, K.A., Smith, J.G., Connell, J.W. and Yokota, R., 2002. Polyimides from 2,3,3',4'-Biphenyltetracarboxylic Dianhydride and Aromatic Diamines. Polymer. 43, 5077-5093.

Holzapfel, G.A., 2000. Nonlinear Solid Mechanics: A Continuum Approach for Engineering. John Wiley & Sons, Ltd., West Sussex, England.

Hu, Y.H. and Sinnott, S.B., 2004. Molecular Dynamics Simulations of Polyatomic-Ion Beam Deposition-Induced Chemical Modification of Carbon Nanotube/Polymer Composites. Journal of Materials Chemistry. 14, 719-729.

Jiang, M., Jasiuk, I. and Ostoja-Starzewski, M., 2002. Apparent Elastic and Elastoplastic Behavior of Periodic Composites. International Journal of Solids and Structures. 39, 199-212.

Jorgensen, W.L., Maxwell, D.S. and Tirado-Rives, J., 1996. Development and Testing of the OPLS All-Atom Force Field on Conformational Energetics and Properties of Organic Liquids. Journal of the American Chemical Society. 117, 11225-11236.

Kaminsky, G.A., Friesner, R.A., Tirado-Rives, J. and Jorgensen, W.L., 2001. Evaluation and Reparametrization of the OPLS-AA Force Field for Proteins via Comparison with Accurate Quantum Chemical Calculations on Peptides. Journal of Physical Chemistry B. 105, 6474-6487.

Leach, A.R., 2001. Molecular Modelling: Principles and Applications. Prentice Hall, New York.

Liang, Z., Gou, J., Zhang, C., Wang, B. and Kramer, L., 2004. Investigation of Molecular Interactions Between (10,10) Single-Walled Nanotube and Epon 862 Resin/DETDA Curing Agent Molecules. Materials Science and Engineering A. 356, 228-234.

Lordi, V. and Yao, N., 2000. Molecular Mechanics of Binding in Carbon-Nanotube-Polymer Composites. Journal of Materials Research. 15, 2770-2779.

Malvern, L.E., 1969. Introduction to the Mechanics of a Continuous Medium. Prentice-Hall, Inc., Upper Saddle River, NJ.

Marsden, J.E. and Hughes, T.J.R., 1994. Mathematical Foundations of Elasticity. Dover Publications, Inc., Mineola, NY.

Nocedal, J. and Wright, S.J., 1999. Numerical Optimization. Springer-Verlag, New York.

Odegard, G.M., Clancy, T.C. and Gates, T.S., 2005. Modeling the Mechanical Properties of nanoparticle/polymer composites. Polymer. 46, 553-562.

Odegard, G.M., Frankland, S.J.V. and Gates, T.S., 2005. Effect of Nanotube Functionalization on the Elastic Properties of Polyethylene Nanotube Composites. AIAA Journal. 43, 1828-1835.

Odegard, G.M., Frankland, S.J.V., Herzog, M.N., Gates, T.S. and Fay, C.C., 2004. Constitutive Modeling of Crosslinked Nanotube Materials. 45th AIAA/ASME/ASCE/AHS/ASC Structures, Structural Dynamics, and Materials Conference, Palm Springs, CA.

Odegard, G.M., Gates, T.S., Nicholson, L.M. and Wise, K.E., 2002. Equivalent-Continuum Modeling of Nano-Structured Materials. Composites Science and Technology. 62, 1869-1880.

Odegard, G.M., Gates, T.S., Wise, K.E., Park, C. and Siochi, E., 2003. Constitutive Modeling of Nanotube-Reinforced Polymer Composites. Composites Science and Technology. 63, 1671-1687.

Ogden, R.W., 1997. Non-Linear Elastic Deformations. Dover Publications, Inc., Mineola, NY.

Ott, K.H. and Meyer, B., 1996. Parametrization of GROMOS Force Field for Oligosaccharides and Assessment of Efficiency of Molecular Dynamics Simulations. Journal of Computational Chemistry. 17, 1068-1084.

Ponder, J.W., 2004, TINKER - Software Tools for Molecular Design. Ver 4.2. Washington University School of Medicine, St. Louis, MO.

Sane, S.B., Cagin, T., Knauss, W.G. and Goddard, W.A., 2002. Molecular Dynamics Simulations to Compute the Bulk Response of Ammorphous PMMA. Journal of Computer-Aided Materials Design. 8, 87-106.

Schroder, J. and Neff, P., 2003. Invariant Formulation of Hyperelastic Transverse Isotropy Based on Polyconvex Free Engery Functions. International Journal of Solids and Structures. 40, 401-445.

Shenogin, S. and Ozisik, R., 2005. Simulation of Plastic Deformation in Glassy Polymers: Atomistic and Mesoscale Approaches. Journal of Polymer Science Part B: Polymer Physics. 43, 994-1004.

Srinivas, S., Caputo, F.E., Graham, M., Gardner, S., Davis, R.M., McGrath, J.E. and Wilkes, G.L., 1997. Semicrystalline Polyimides Based on Controlled Molecular Weight Phthalimide End-Capped 1,3-Bis(4-Aminophenoxy)Benzene and 3,3',4,4'-Biphenyltetracarboxylic Dianhydride: Synthesis, Crystallization, Melting, and Thermal Stability. Macromolecules. 30, 1012-1022.

Sun, C.T. and Vaidya, R.S., 1996. Prediction of Composite Properties from a Representative Volume Element. Composites Science and Technology. 56, 171-179.

Sun, H., 1998. COMPASS: An ab Initio Force-Field Optimized for Condensed-Phase Applications - Overview with Details on Alkane and Benzene Compounds. Journal of Physical Chemistry B. 102, 7338-7364.

Tersoff, J., 1988. Empirical Interatomic Potential for Carbon, with Applications to Amorphous Carbon. Physical Review Letters. 61, 2879-2882.

Tersoff, J., 1988. New Empirical Approach for the structure and energy of covalent systems. Physical Review B. 37, 6991-7000.

Theodorou, D.N. and Suter, U.W., 1986. Atomistic Modeling of Mechanical Properties of Polymeric Glasses. Macromolecules. 19, 139-154.

Truesdell, C. and Noll, W., 2004. The Non-Linear Field Theories of Mechanics. Springer-Verlag, New York.

Table I. Values of deformation parameters

Deformation parameters	Value (unitless)	Finite-valued strain components
α_1	1.002497	$E_{11} = E_{22} = E_{33} = 0.25\%$
α_2	1.002485	$E_{11} = E_{22} = E_{33} = 0.50\%$
α_3	1.002472	$E_{11} = E_{22} = E_{33} = 0.75\%$
α_4	1.002460	$E_{11} = E_{22} = E_{33} = 1.00\%$
β_1	0.001249	$\gamma_{23} = \gamma_{13} = \gamma_{12} = 0.25\%$
β_2	0.001246	$\gamma_{23} = \gamma_{13} = \gamma_{12} = 0.50\%$
β_3	0.001243	$\gamma_{23} = \gamma_{13} = \gamma_{12} = 0.75\%$
β_4	0.001240	$\gamma_{23} = \gamma_{13} = \gamma_{12} = 1.00\%$

Table II. Predicted material parameters of the polymers from static molecular simulations (all parameters have units of Pa)

Material	c_1	c_2
Polycarbonate (AMBER force field)	2.23×10^{9}	2.58×10^{7}
Polycarbonate (OPLS-AA force field)	1.81×10^{7}	4.29×10^{6}
Polycarbonate (MM3 force field)	1.41×10^{9}	1.17×10^{6}
Polyimide (AMBER force field)	9.64×10^{8}	4.92×107^{7}
Polyimide (OPLS-AA force field)	1.58×10^{9}	1.82×10^{7}
Polyimide (MM3 force field)	1.52×10^{9}	3.43×10^{6}

Table III. Predicted material parameters of the polymers from dynamic molecular simulations (all parameters have units of Pa)

Material	c_1	c_2
Polycarbonate (AMBER force field)	2.44×10^{9}	6.69×10^{7}
Polycarbonate (OPLS-AA force field)	2.00×10^{8}	1.62×10^{8}
Polycarbonate (MM3 force field)	2.28×10^{8}	2.09×10^{8}
Polyimide (AMBER force field)	6.08×10^{8}	2.32×10^{8}
Polyimide (OPLS-AA force field)	1.58×10^{9}	2.13×10^{8}
Polyimide (MM3 force field)	1.16×10^{9}	1.32×10^{8}

Table IV. Predicted and Experimental Elastic Properties of Polycarbonate

Method	**Young's Modulus (GPa)**	**Shear Modulus (GPa)**
Experiment	2.2	0.8
AMBER force field (static simulation)	4.0	1.4
OPLS-AA force field (static simulation)	0.3	0.2
MM3 force field (static simulation)	0.2	0.1
AMBER force field (dynamic simulation)	9.4	3.7
OPLS-AA force field (dynamic simulation)	4.1	9.1
MM3 force field (dynamic simulation)	4.7	11.7

Table V. Predicted and Experimental Elastic Properties of Polyimide

Method	Young's Modulus (GPa)	Shear Modulus (GPa)
Experiment	3.6	1.3
AMBER force field (static simulation)	6.1	2.8
OPLS-AA force field (static simulation)	2.8	1.0
MM3 force field (static simulation)	0.6	0.2
AMBER force field (dynamic simulation)	10.6	13.0
OPLS-AA force field (dynamic simulation)	18.4	11.9
MM3 force field (dynamic simulation)	12.3	7.4

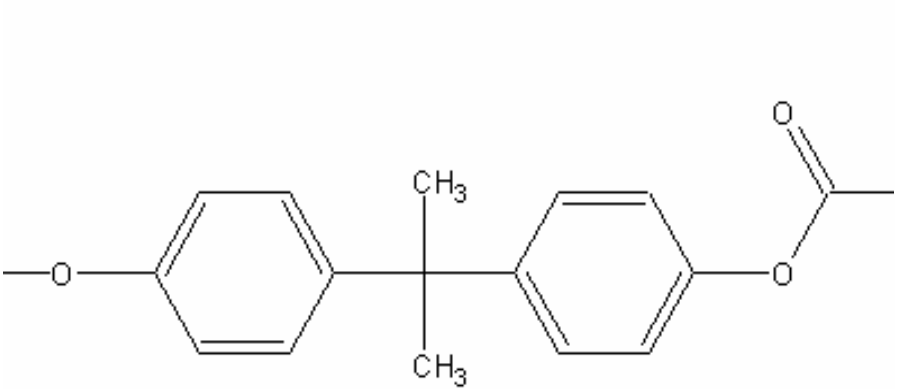

Figure 1. Schematic illustration of the polycarbonate monomer unit

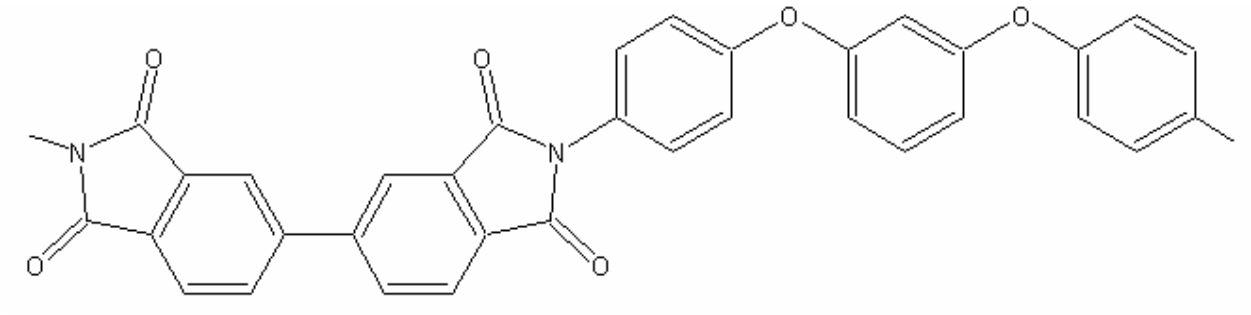

Figure 2. Schematic illustration of the BPDA (1,3,4) APB polyimide monomer unit

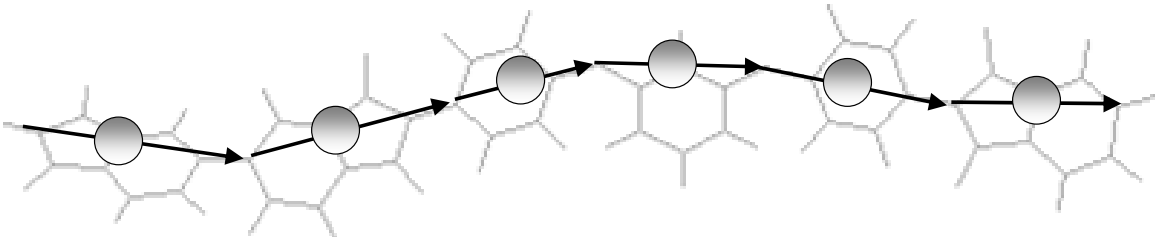

Figure 3. Depiction of the mapping of the atomistic polymer model to the coarse-grained linked vector model

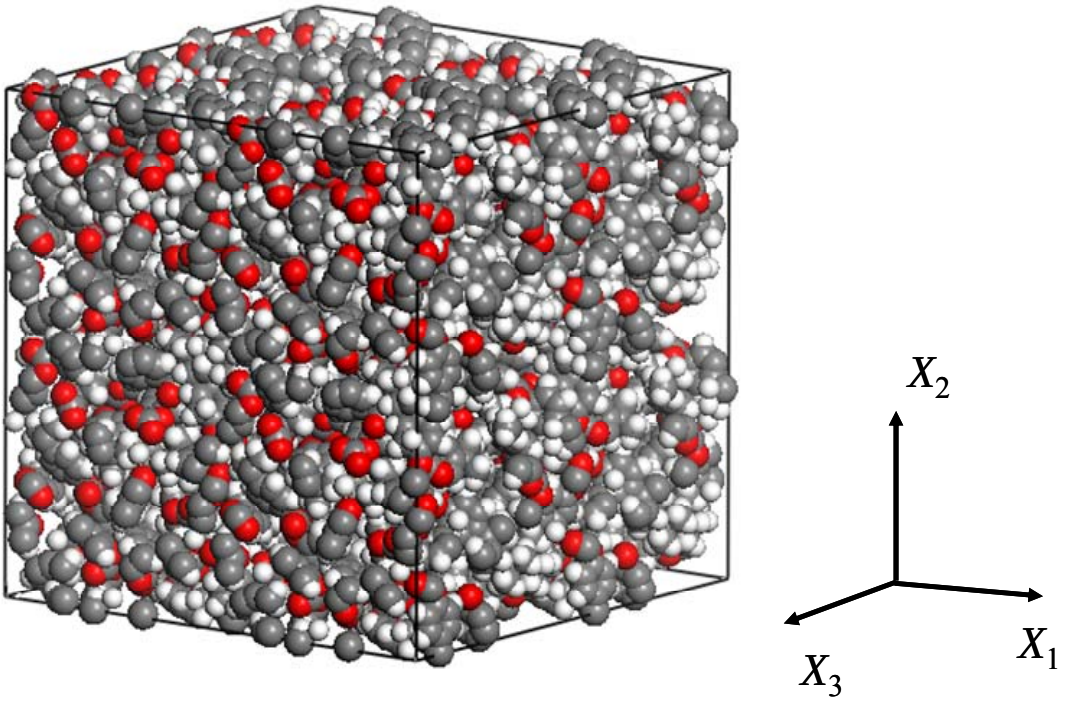

Figure 4. RVE of the polycarbonate material

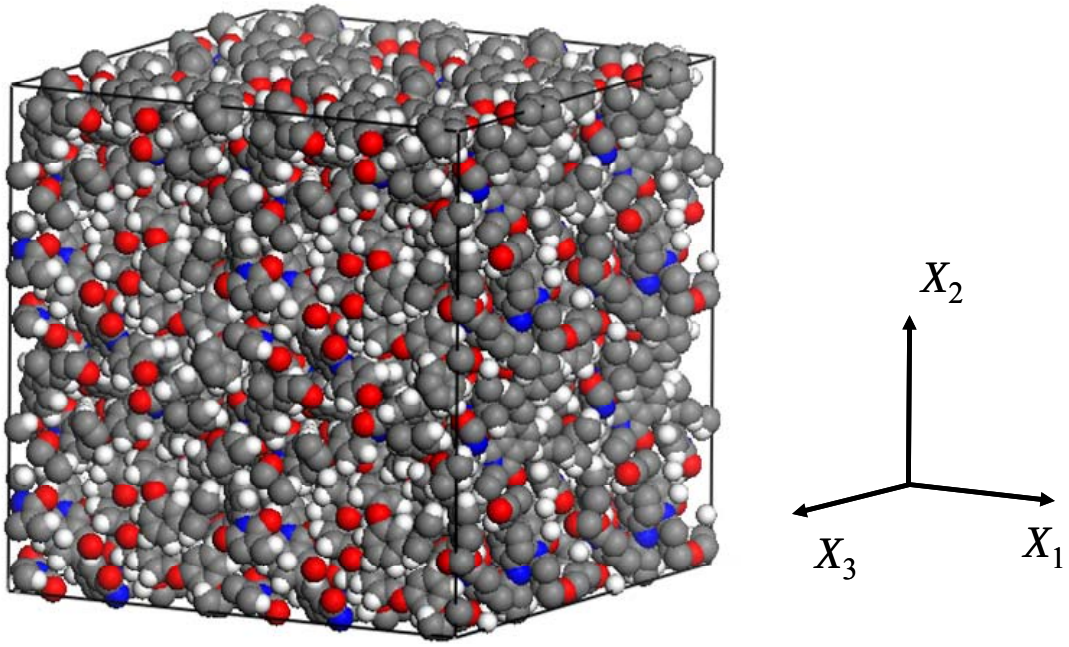

Figure 5. RVE of the polyimide material

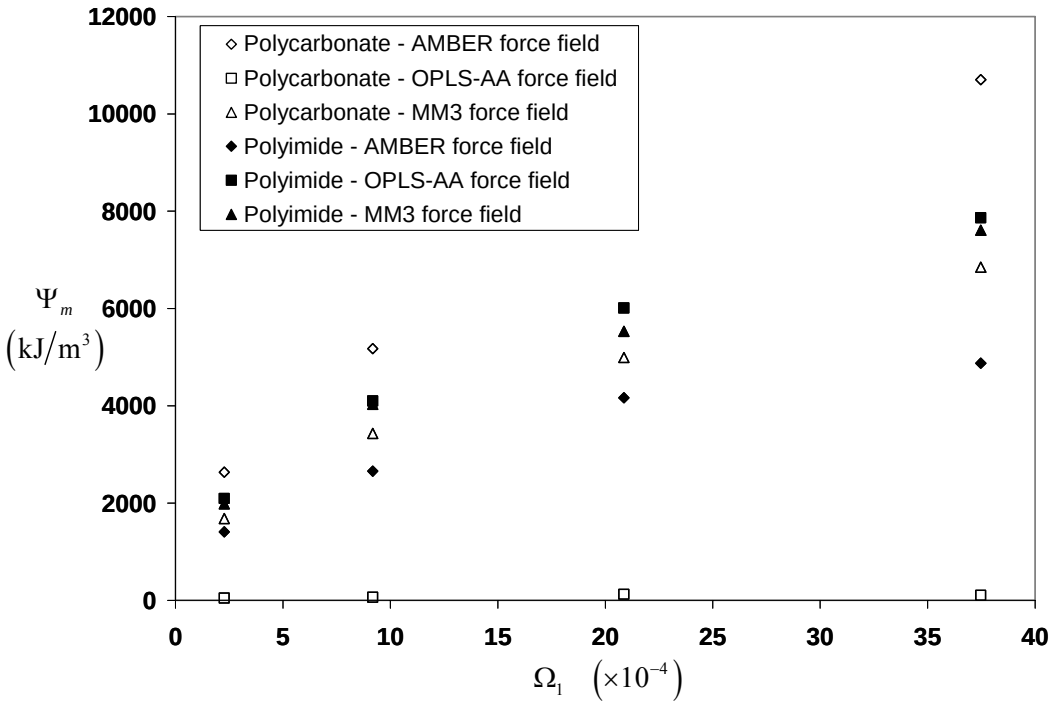

Figure 6. Simulated molecular strain-energy density for volumetric deformation with static molecular simulations

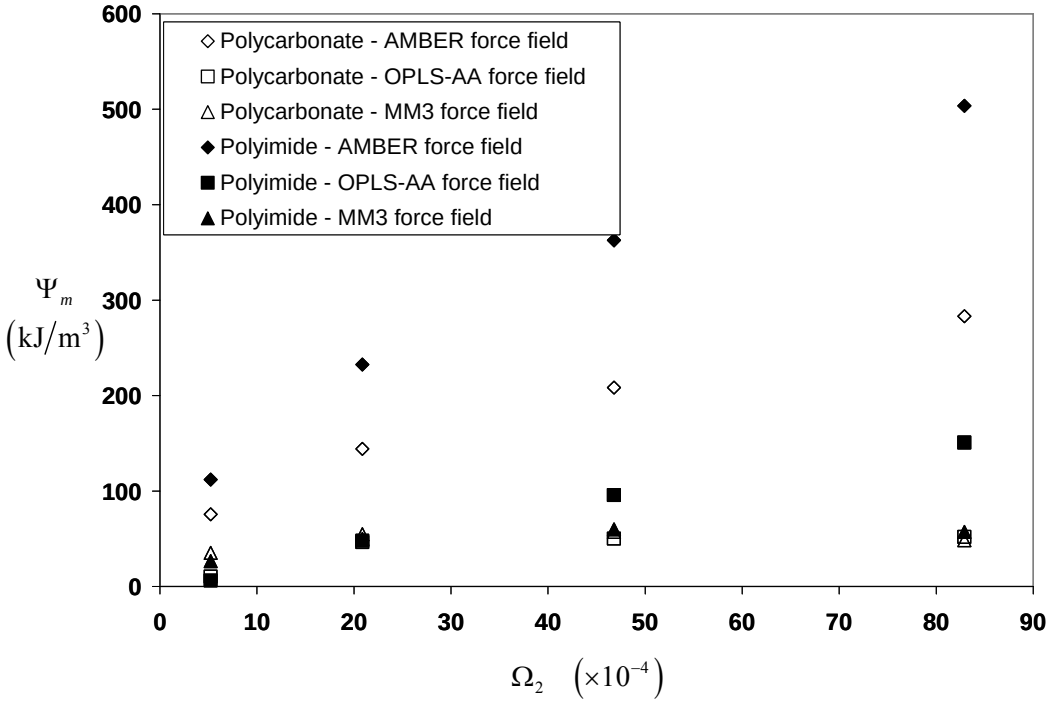

Figure 7. Simulated molecular strain-energy density for isochoric deformation with static molecular simulations

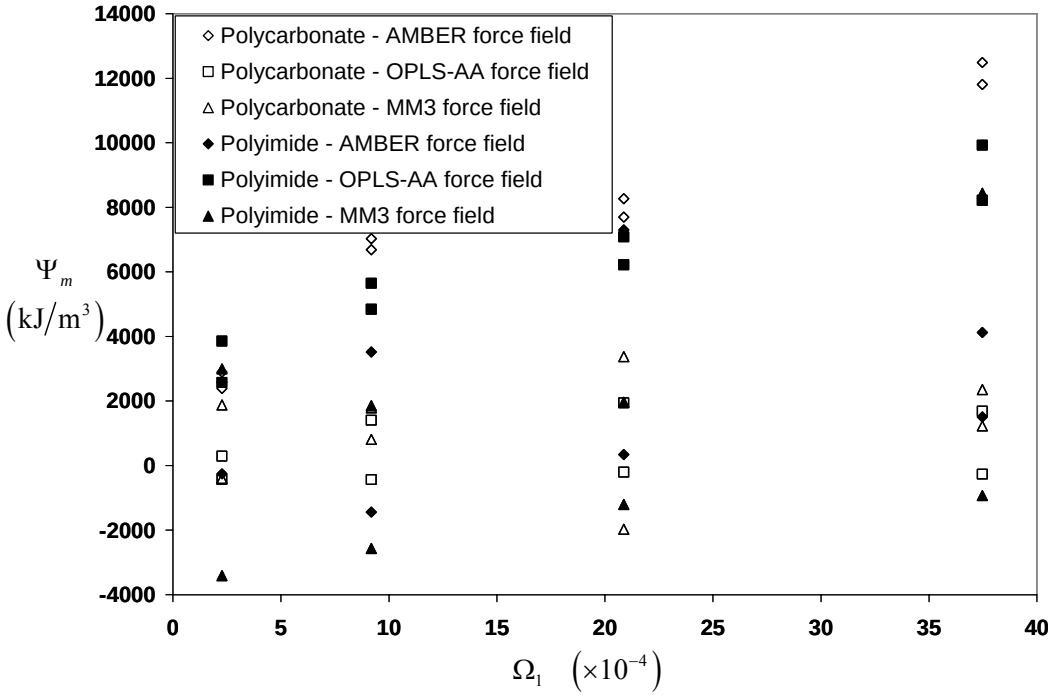

Figure 8. Simulated molecular strain-energy density for volumetric deformation with dynamic molecular simulations

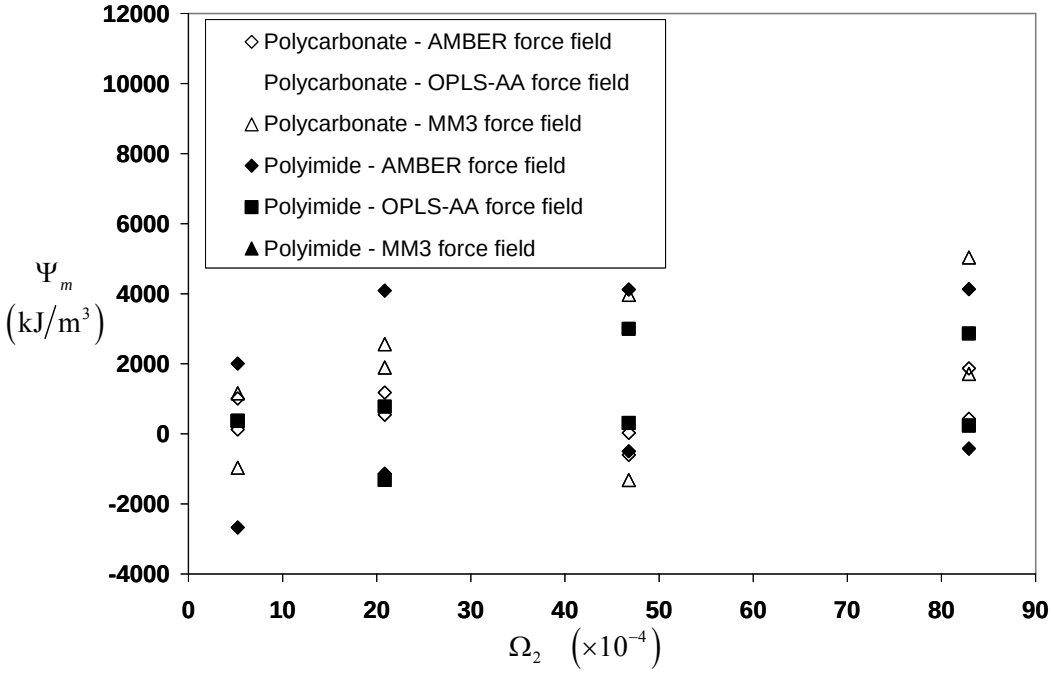

Figure 9. Simulated molecular strain-energy density for isochoric deformation with dynamic molecular simulations

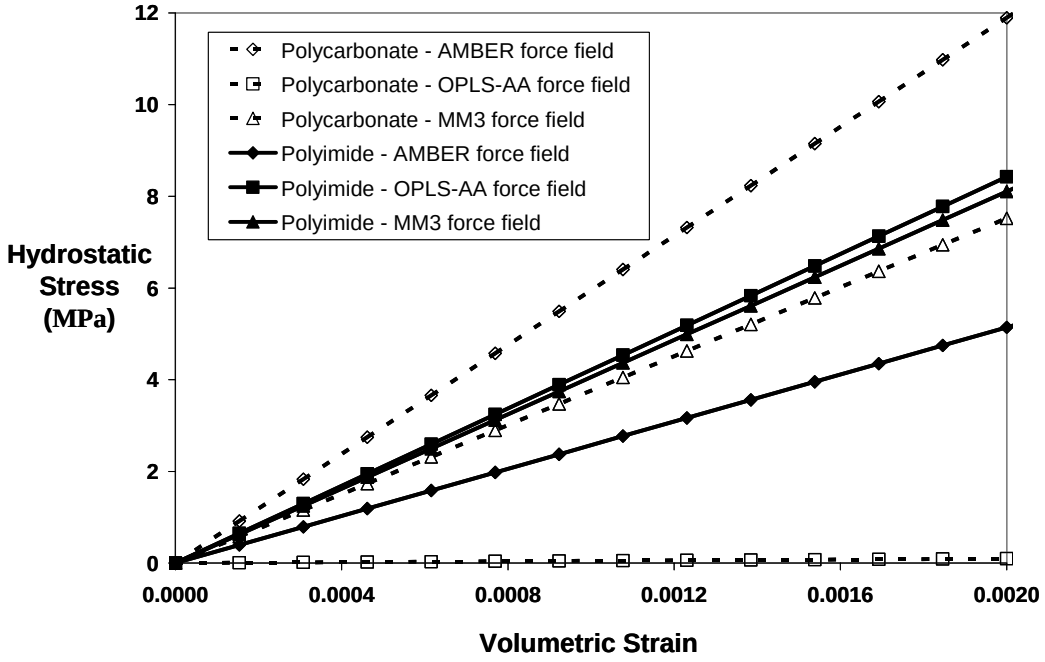

Figure 10. Predicted hydrostatic stress versus volumetric strain behavior for the material parameters determined with the static molecular simulations

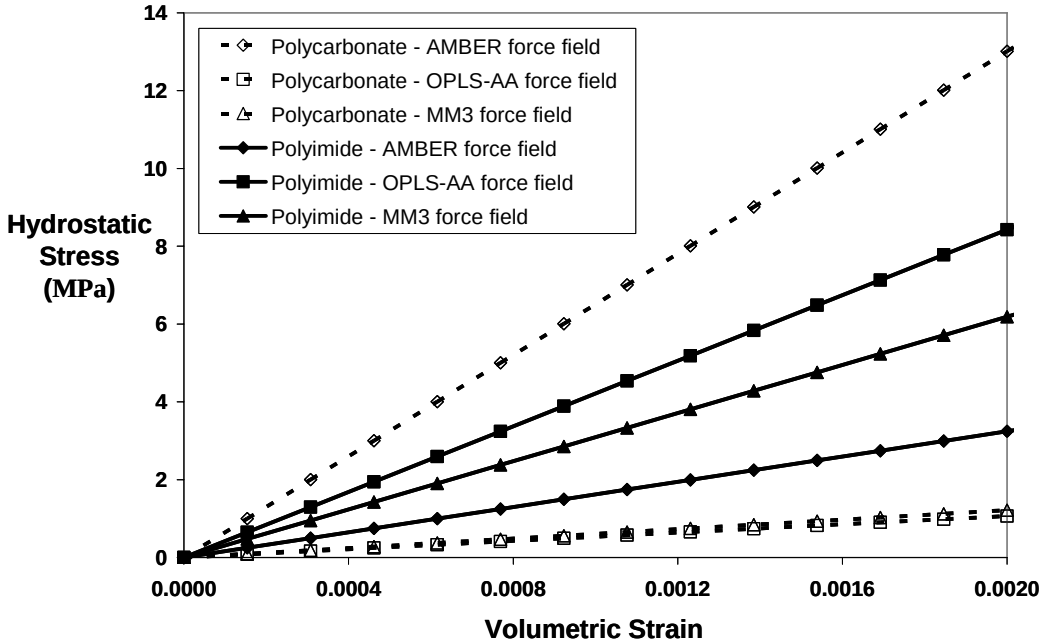

Figure 11. Predicted hydrostatic stress versus volumetric strain behavior for the material parameters determined with the dynamic molecular simulations

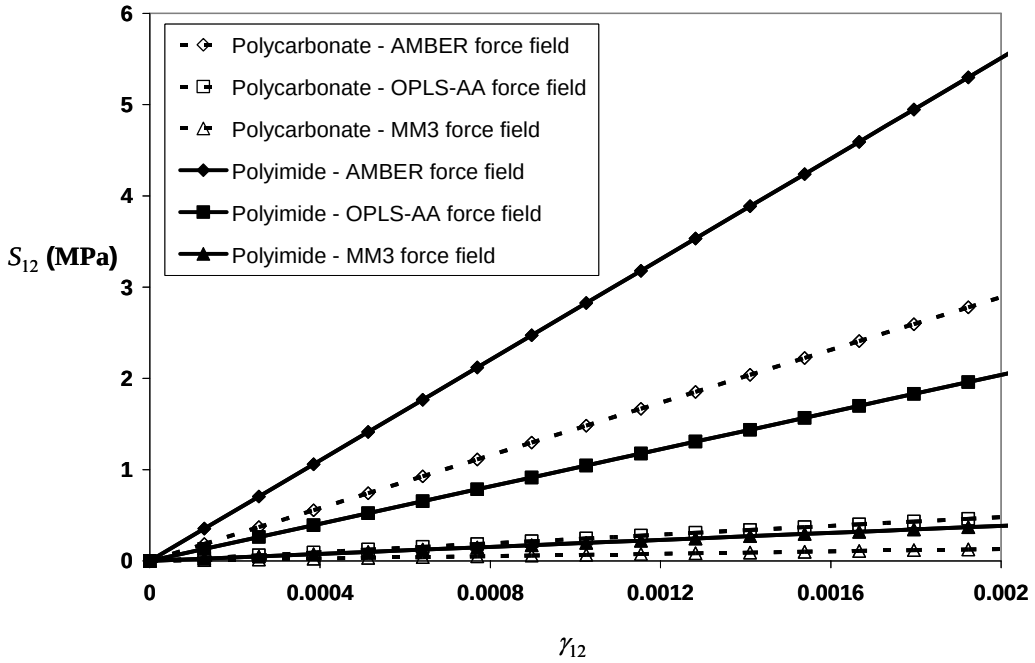

Figure 12. Predicted shear stress versus shear strain behavior for the material parameters determined with the static molecular simulations

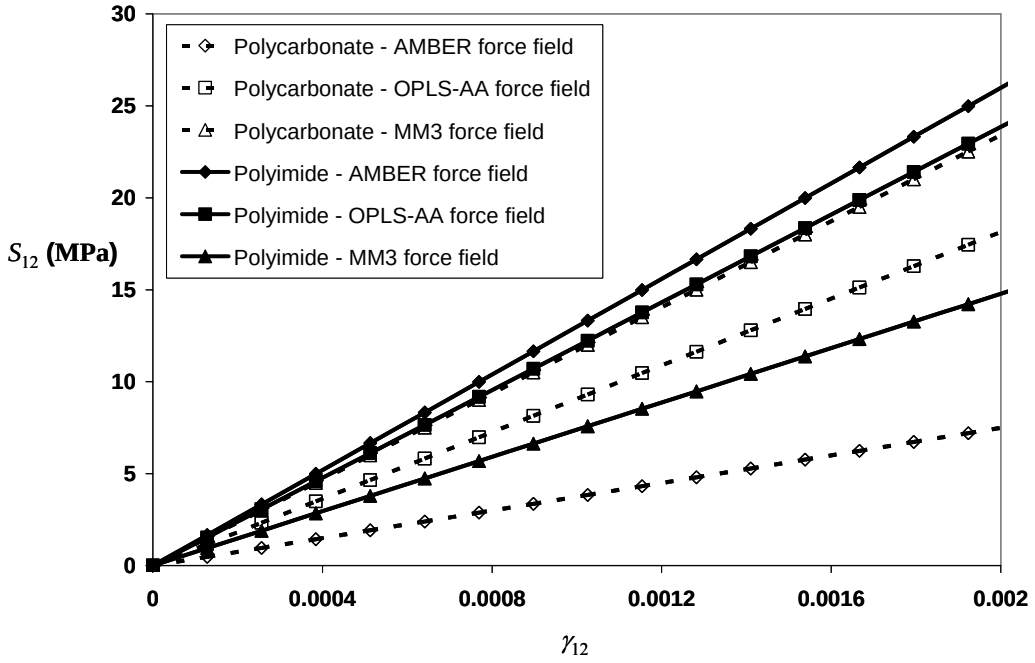

Figure 13. Predicted shear stress versus shear strain behavior for the material parameters determined with the dynamic molecular simulations